

Detection of Nanoscale Magnetic Activity Using a Single Carbon Nanotube

Caterina Soldano,^{*,†,||} Swastik Kar,^{*,†,||} Saikat Talapatra,[§]
Saroj Nayak,[†] and Pulickel M. Ajayan[⊥]

Department of Physics, Applied Physics and Astronomy, Rensselaer Polytechnic Institute, Troy, New York 12180, Department of Mechanical Engineering and Materials Science, Rice University, Houston, Texas 77006, and Department of Physics, Southern Illinois University Carbondale, Carbondale, Illinois 62901

Received August 12, 2008; Revised Manuscript Received October 6, 2008

ABSTRACT

The ultimate conductometric sensor for ferromagnetic activity of nanoscale magnetic materials could be a single carbon nanotube. We show that the electrical conductance of an individual carbon nanotube is sensitive to magnetic transitions of nanoscale magnets embedded inside it. To establish this, multiwall carbon nanotubes were impregnated with cobalt nanoclusters. Temperature dependence of conductance ($5\text{ K} < T < 300\text{ K}$) of these nanotubes shows the usual Luttinger-liquid power law behavior at higher temperatures and an onset of Coulomb blockade at lower temperatures. At the lowest temperature ($T \sim 6\text{ K}$), the differential conductance (dI/dV versus V) develops aperiodic fluctuations under an external magnetic field B , the rms amplitude of which grows with the magnitude of the field itself. Low-temperature magnetoconductance, studied as function of temperature and bias, can be interpreted in terms of weak antilocalization effects due to the presence of the magnetized clusters. The temperature dependence of magnetoconductance further presents a “peak”-like feature and slow dynamics around $T = 55\text{ K}$, which depend on the magnitude and history of the applied B field. These observations indicate a sensitivity of electronic transport in the multiwall nanotubes to the dynamics of nanoscale magnets at low temperature.

The electronic properties of carbon nanotubes¹ remain one of the most exciting areas of research in nanoscale condensed matter, due to the exotic interplay of ballistic transport,² strong electron–electron interactions,^{3,4} Coulomb blockade and single charge transport,⁵ and possible spin–orbit coupling⁶ in a one-dimensional confined geometry. Recent progresses in the controlled injection, manipulation, and detection of carrier spin using ferromagnetic electrodes^{7–9} in carbon nanotubes have generated additional excitement in this field. While spin-polarized electrons retain their polarization over hundreds of nanometers¹⁰ in clean carbon nanotubes, a fundamental issue of considerable importance is to understand how unpolarized electrons behave as they travel in the proximity of strong local magnetic fields. In

the past, the presence of dilute magnetic impurities on a carbon nanotube host has been shown to give rise to the Kondo effect, as a result of the interaction between the electron of the host tube and the spin of the magnetic impurity (cobalt) on the tube itself.^{11,12} Other works have proposed that the presence of ferromagnetic materials in the vicinity of the electron wave function can significantly modify the density of states (DoS) of the carbon nanotube^{13,14} and can give rise to enhanced spin–orbit coupling effects.¹⁵ It is important to experimentally investigate these and other properties when nanoscale ferromagnetic materials are placed in the vicinity of carbon nanotubes. In addition, if the ferromagnetic materials undergo any magnetic transition, the question arises about how these changes affect the charge transport in carbon nanotubes, and if such phenomena can be experimentally detected.

In this Letter, we present the fabrication of individual multiwall carbon nanotubes embedded with cobalt nanoclusters (Co-MWNT) inside the tubes, and the investigation of their low-temperature transport properties through measurement of conductance (G) over a range of temperatures ($5\text{ K} < T < 300\text{ K}$), applied bias ($0\text{ mV} < V < 100\text{ mV}$), and magnetic field ($0\text{ T} < B < 5\text{ T}$). It is important to mention that the nanoclusters, which are a few nanometers

* To whom correspondence should be addressed. E-mail: csoldano@cemes.fr (C.S.); kars@rpi.edu (S.K.). Present address for C.S.: CEMES – Centre d’Elaboration de Matériaux et d’Etudes Structurales, CNRS – UPR 8011, 29 Rue Jeanne Marvig, BP 94347, 31055 Toulouse, Cedex 4, France. Telephone: (+33) (0)5 62 25 78 65 (C.S.). Fax: (+33) (0)5 62 25 79 99 (C.S.).

[†] Department of Physics, Applied Physics and Astronomy, Rensselaer Polytechnic Institute.

[§] Southern Illinois University Carbondale.

^{||} These authors contributed equally.

[⊥] Department of Mechanical Engineering and Materials Science, Rice University, Houston, Texas 77006.

to tens of nanometers in size, are neither large enough (compared to bulk ferromagnetic contacts), such that they can completely polarize the electron spins, nor small enough to be considered impurities, such as those that can give rise to the Kondo effect. In addition, since charge transport in multiwalled carbon nanotubes is known to be limited to the outer walls,¹⁶ and the Co clusters in our system are embedded inside the nanotube rather than on the outer surface, they do not provide elastic scattering sites like defects do. From a fundamental point of view, these hybrid nanostructures, hence, belong to a new class of magnetic material.

The introduction of metals or metal carbide and oxide in carbon nanotubes has been demonstrated to significantly alter their electronic and mechanical properties.^{17,18} The nanotube shells protect the inner metal clusters against oxidation and enhance their long-term stability.¹⁹ In addition to fundamental physics, nanotubes filled with ferromagnetic materials such as iron, cobalt, or nickel have gained considerable interest due to their potential applications in magnetic data storage technology due to their small size and enhanced magnetic coercivity.¹⁹ Partially or fully filled carbon nanotubes (CNTs) also have a variety of other industrial applications such as catalysts,²⁰ electronic devices, and biosensors.²¹ To achieve this, various techniques for encapsulating metals, metal oxides, and chlorides in multiwall or single wall carbon nanotubes have been developed such as ion-beam sputtering,²² arc-discharge technique,^{23,24} chemical vapor deposition (CVD) techniques,^{25,26} and high-temperature treatment.²⁷

In contrast with the previously mentioned methods, we have adopted an electrochemical route to embed ferromagnetic nanoclusters inside carbon nanotubes that were previously grown inside anodized alumina templates. This approach allows selective deposition of metallic clusters on the inner volume of the nanotubes, leaving the outer walls free of any metallic impurities. It also allows us to fabricate devices out of individual nanotubes after the metal impregnation.

Multiwall carbon nanotubes (MWNTs) were first grown inside nanoporous anodized alumina templates (pore diameter $\sim 250\text{--}300$ nm) using chemical vapor deposition of acetylene gas at the temperature of approximately 650°C . Figure 1a shows the top part of one such template, after tubes were partly exposed using a dilute NaOH etching solution. This exposed side of the template was then metalized with thermally evaporated silver. The metalized template was laid on a conducting substrate and masked with an insulating material in order to leave a partially exposed unmetalized surface of the membrane. This electrode was then immersed in a cobalt sulfate-based electrolyte solution where the MWNTs act as the working electrode, as shown in the schematic in Figure 1b. This way, the silver film and the carbon nanotubes formed an array of extended electrodes, with only the inner surface of the nanotubes exposed to the electrolyte. Electrodeposition was used to introduce cobalt clusters inside each tube. After the deposition, the template was dissolved using NaOH to release the metal-embedded structures. Figure 1c shows a scanning electron microscopy (SEM) image of partially released Co nanocluster impreg-

nated MWNTs, and part d shows a bright field (BF) transmission electron microscopy (TEM) image of an individual Co nanocluster impregnated MWNT. The size of the Co clusters (lighter and darker contrasts in the SEM and TEM images, respectively) was found to vary between a few nanometers to hundreds of nanometers depending on the deposition time. In particular, the structures shown in Figure 1c correspond to a growth time of about ~ 25 min, with cluster size of approximately $50\text{--}100$ nm. The released nanotubes were washed, dispersed in isopropyl alcohol, and then spin-cast on Si/SiO₂ substrates with photolithographically prepatterned electrodes. Figure 1e shows a typical magnetic force microscopy (MFM) image of an individual tube when dispersed on the substrate, where lighter locations indicate the magnetic response due to the presence of the Co nanoclusters. Two-probe individual devices were fabricated using focus ion beam (FIB) lithography to attach platinum leads between the nanotubes and the prefabricated electrodes (Figure 1f). Pristine devices, embedded with *randomly* magnetized Co clusters, are referred to as *nm*-Co-MWNTs, whereas devices that were exposed to magnetic fields (up to $B = 5$ T) could be expected to have their clusters magnetized in the direction of the applied field. Such devices showed marked differences in their transport properties, and they will be referred to as *m*-Co-MWNTs. The difference in transport between *nm*-Co-MWNTs and *m*-Co-MWNTs suggests that the transport mechanism is sensitive to the relative orientations of the cluster magnetizations.

Template-grown MWNTs are usually disordered and hence have larger two-terminal resistances compared to arc-grown carbon nanotubes. Hence, for our transport measurements, we selected short ($< 1\ \mu\text{m}$) devices with comparatively lower resistances. At room temperature, these devices showed linear current–voltage characteristics with typical two-terminal resistances of a few k Ω , indicating low-resistance ohmic contacts. Figure 2 shows the temperature dependence of the low-bias ($= 1$ mV) linear conductance G of an *nm*-Co-MWNT device of length $L \sim 800$ nm. The entire temperature range ($5\text{--}300$ K) can be divided into two regions, each following approximate power laws as denoted by the solid and the dashed lines in the log–log plot. The inset in Figure 2 shows the bias dependence of the differential conductance dI/dV at $T = 6$ K. We find $G(T) \propto T^\alpha$ for $eV/k_B T \ll 1$ and $dI/dV(V) \propto V^\alpha$ for $eV/k_B T \gg 1$, with a value of $\alpha \sim 0.258$, indicating that the *nm*-Co-MWNTs behaved as Luttinger liquids.¹⁶ Multiwall carbon nanotubes can be considered to be multichannel Luttinger liquids,^{28,29} and in the high-temperature limit the conductivity can be expressed as $\sigma(T) = Nv_F\tau_0(2e^2/h)(2\pi e^{1+C})^\alpha [k_B T/\hbar\omega_c]^\alpha$, where v_F is the Fermi velocity, ω_c is the ultraviolet cutoff frequency, τ_0 is the scattering mean free time, $C = 0.577$ is the Euler constant, k_B is the Boltzmann constant, and N represents the number of conducting channels. Assuming $v_F = 8 \times 10^5$ ms⁻¹,³⁰ we estimate that the nanotube has $N = 6$ quantum channels with a mean free path $l_e \sim 170$ nm and a large value of the scattering time ($\sim 2 \times 10^{-12}$ s).

The log–log plot of the temperature dependence of G shows a change in slope at an approximate temperature of

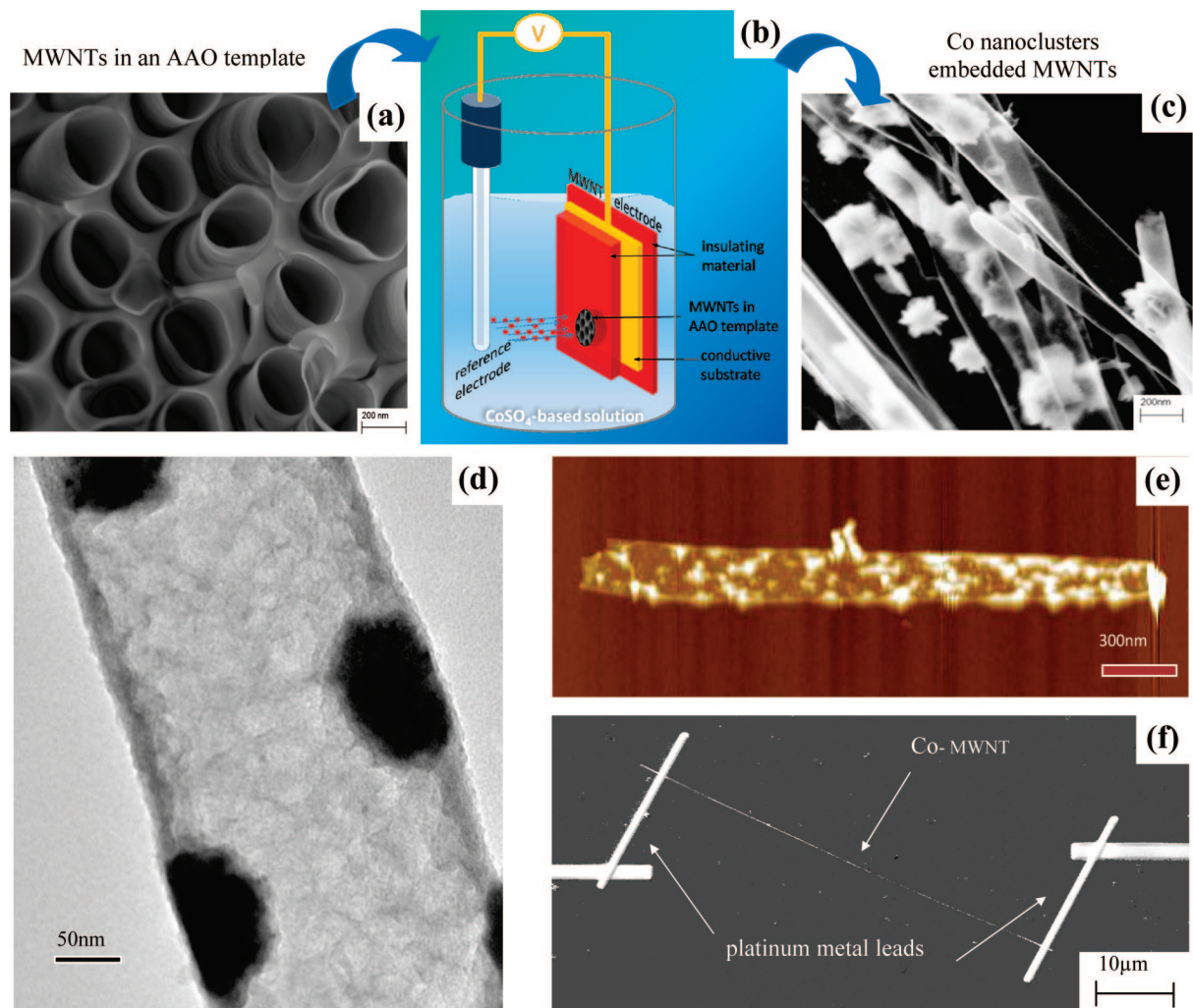


Figure 1. (a) Bare MWNTs grown inside an AAO template; the template has been partially etched to expose the nanotubes for imaging. (b) Schematic of the electrodeposition setup. (c) SEM image of a bundle of Co nanocluster filled MWNTs after electrodeposition, where lighter contrast areas show the nanoclusters inside the MWNTs. (d) Bright field TEM image of an individual Co filled MWNT, where darker spots correspond to the clusters. (e) MFM image of a cobalt filled tube, where lighter spots represent the magnetic response due to the presence of the Co clusters in the tube. (f) Co filled two-probe MWNT device on SiO₂/Si substrate; leads are fabricated by FIB lithography.

35 K, as shown in Figure 2, where the solid and dashed lines intercept each other in the figure. In carbon nanotubes, a change of exponent in the power law dependence of G versus T has been previously reported.³¹ This phenomenon has been interpreted in terms of an effective and unconventional Coulomb blockade (CB) as a result of tunneling into an interacting disordered metal, leading to a Luttinger-liquid-like zero-bias anomaly. For a nanotube of radius R , the exponent α is given by $\alpha = (R/2\pi\hbar D\nu_0) \ln(1 + \nu_0 U_0)$, where D is the diffusion coefficient, $\nu_0 = (M/2\pi\hbar\nu_F)$ is the noninteracting density of states, and U_0 is an effective short-ranged 1D interaction potential. In this case, $M (= 2N + 1)$ is the number of spin degenerate modes. For $N = 6$, we estimate $\alpha = 0.22$, which is close to our experimental finding. We conclude that the host MWNT is a low-disorder (disorder density $L/l_c \sim 5$) multichannel Luttinger liquid, with onset of an unconventional Coulomb blockade at low temperatures. These observations are in agreement with past works, and hence, we also conclude that, in the nm -Co-MWNTs, the

randomly magnetized Co clusters do not contribute significantly to the charge transport in the hybrid device.

The initial set of experiments was performed in the absence of any magnetic field. Thereafter, the differential conductance, dI/dV , was measured as function of bias at $T = 6$ K for a range of magnetic fields between 0 and 5 T in incremental steps of $\Delta B = 25$ mT, applied perpendicular to the tube axis (as shown in the schematic in Figure 3). Exposing the devices to the applied fields at low temperatures can be expected to magnetically align the Co clusters at the end of the experiment, and the MWNT devices can then be designated as an m -Co-MWNT device. Figure 3a shows a color contour plot of the differential conductance as a function of bias and magnetic fields. We find that, for small magnetic fields, the differential conductance evolves smoothly as a function of bias. With increasing B , sharp fluctuations appear in the dI/dV versus V curves. To bring this out clearly, we have plotted dI/dV versus V for representative values of B , shown in Figure 3b. Each of these curves has been shifted

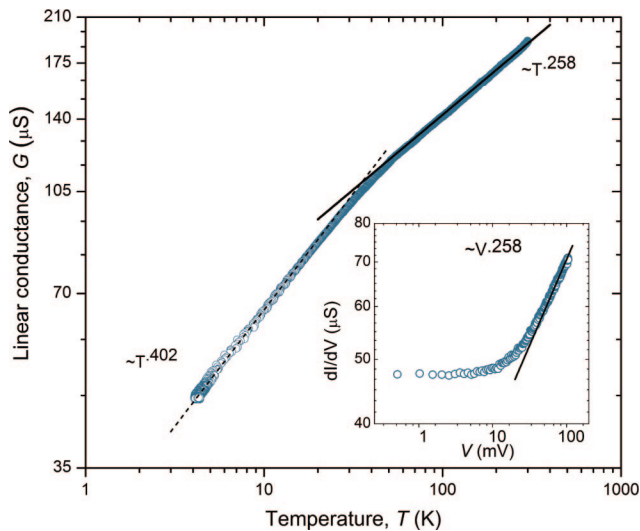


Figure 2. Conductance as a function of the temperature and (inset) bias at $T = 6$ K for a nonmagnetized Co-MWNT. In the higher energy (temperature or bias) limit, Luttinger-liquid type power law dependences are found. A change in the slope of the exponent in G versus T suggests the onset of Coulomb blockade.

horizontally by intervals of $\sim 5 \mu\text{S}$ for clarity. With increasing magnetic field, fluctuations appear in the dI/dV versus V curves with no symmetry of the oscillations with respect to the zero-bias value. No data averaging or smoothening has been performed to preserve the full extent of those oscillations. We note that such fluctuations in the differential conductance in MWNTs with an applied magnetic field have never been reported in the past and were completely absent in our own experiments with bare MWNTs without any embedded clusters. It can be seen that the fluctuation in the curves grows in amplitude with increasing B . To quantify this further, the rms fluctuations, $\Delta G_{\text{rms}}(B) = (\langle (dI/dV[V, B] - dI/dV[V, B = 0])^2 \rangle_V)^{1/2}$, have been plotted as a function of B in Figure 3c. We find that the rms fluctuations continue to grow with increasing B up to the maximum value of 5 T, as shown in Figure 3c. To eliminate the possibility that these fluctuations arise from time dependent conductance fluctuations, we have measured the rms fluctuations in $G = G(t)$ at representative values of V and B over the entire range of experiments and found this to be orders of magnitude smaller (~ 20 nS) than $\Delta G_{\text{rms}}(B)$ and independent of V and B . In addition, fluctuations in magnetoconductance (G versus B , discussed later) curves for fixed values of V showed no increasing trend with B . From this, we conclude that the appearance of sharp fluctuations were real oscillations in the differential conductance (dI/dV versus V) of the host MWNTs, and their magnitude grows with increasing ferromagnetic alignment of the Co nanoclusters embedded within them when B is increased.

Fluctuations in the differential conductance are usually associated with the appearance of discrete energy levels in the density of states (DoS) of the material. *Ab initio* calculations of Co impregnation of single wall nanotubes have been shown¹³ to greatly impact the DoS of carbon nanotubes, and the resultant hybrid structures demonstrate substantial magnetism with the appearance of spin-polarized

states near the Fermi level. In multiwall nanotubes, electronic states are very closely placed ($\sim 10\text{--}100 \mu\text{eV}$)³¹ owing to their large diameter, and hence, at $T = 6$ K (with a thermal smear of about 0.5 meV), such states will not be distinguishable. The fluctuations observed are hence smeared out thermally, and the measured dI/dV shows the thermally convolved oscillations. With increasing magnetic fields, as more clusters get oriented magnetically in the same direction, this effect grows in size, resulting in the increase of $\Delta G_{\text{rms}}(B)$ with B . We believe that the oscillations in the m -Co-MWNT system are a signature of an incremental appearance of discrete states superposed on the “unmagnetized” density of states of the nm -Co-MWNT system. Furthermore, we found that subsequent measurement of dI/dV versus V at $B = 0$ T did not bring the device back to its initial “low-fluctuation” state, implying that the density of states of the system underwent a permanent change once the random domains were completely magnetically aligned.

In addition to modifying the differential conductance, the magnetic field decreases the linear conductance by a small (up to $\sim 1\%$) amount. This magnetoconductance (MC) has been measured as a function of measuring bias ($4 \text{ mV} < V < 100 \text{ mV}$). Figure 4a shows the MC curves for $-5 \text{ T} < B < 5 \text{ T}$, for representative biases, for which we find an overall negative magnetoconductance.

Low-temperature MC in carbon nanotubes has been reported previously by several groups. In most cases, the reported MC was shown to be positive and was attributed to a weak localization phenomenon.^{32,33} Negative MC is rather unusual in carbon nanotubes, and we discuss the possible reasons for our observed data. In low-dimensional systems, various mechanisms could give rise to the negative MC at low temperature: two bands conduction,³⁴ e - e interaction,³⁵ correlation in the presence of spins,^{36,37} and weak antilocalization (WAL) as a result of enhanced dominating spin-orbit interaction (SOI).³⁸ A detailed analysis of the temperature dependence of the conductance²⁸ suggests that in our devices the e - e interaction effect begins to play a dominant role for temperatures well below 4 K, a value that is beyond the experimental conditions of the present work. Therefore the influence of e - e interactions, if any, is really weak and does not bring any observable effect into our present measurements. Moreover, the application of a magnetic field in a strongly disordered system in the presence of Coulomb interactions produces the alignment of the spins, leading to a negative and isotropic MC. However, in the present case, the study of the temperature dependence suggests that MWNTs are not strongly disordered systems; in addition, no sign of isotropy is observed in the MC curves. Further, if the second shell participates in the conduction, a saturation of the conductance at low temperature is expected.³⁹ This feature is not observed in the range of temperatures under investigation, suggesting that in the present case there is no additional contribution to the negative MC from a second shell conduction within the experimentally observed temperatures. For the above reasons, we believe that the dominant mechanism that gives rise to

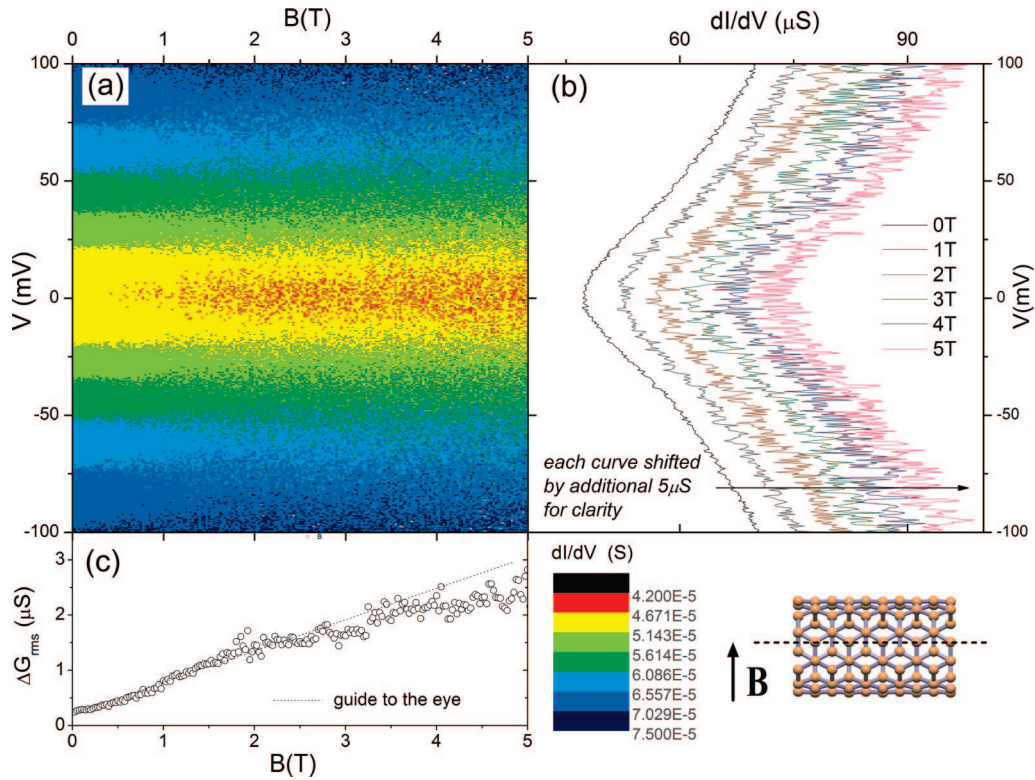


Figure 3. (a) Differential conductance, dI/dV as function of the applied bias for an applied magnetic field $0 < B < 5$ T measured at field intervals $\Delta B = 25$ mT at the temperature of $T = 6$ K. (b) dI/dV versus V curve for representative increasing magnetic fields ($B = 0, 1, 2, 3, 4,$ and 5 T), as indicated by the arrow. Random oscillations appear in those curves with increasing magnetic field. Curves are shifted horizontally by $5 \mu\text{S}$ intervals for clarity. (c) Root-mean-square (see text) of the oscillations' amplitude as a function of the applied magnetic field shows almost a linear dependence on the field. (Bottom right) Orientation of the magnetic field with respect to the nanotube device.

the observed negative MC in our devices is weak antilocalization.

Weak anti localization (WAL) arises when the localization of the electron wave function in the system is progressively destroyed³⁸ as a result of doping, shape asymmetry of the system, presence of impurities, and spin-orbit interaction. The WAL correction to the conductance is given by $\Delta G(B) = -(e^2/48\pi h)(B/H_{in})^2$,³⁸ where B is the magnetic field and H_{in} is the magnetic field at which inelastic scattering starts to dominate the charge transport. Weak antilocalization fits to the MC data provides an estimate of the value of H_{in} and the associated inelastic scattering length scale L_{in} given by $L_{in} = (h/8\pi e H_{in})^{1/2}$. WAL fits (dashed lines) were performed on the MC data as a function of bias and temperature (see later). For our system, estimated values of H_{in} were 3–4 times larger than the maximum applied field ($=5$ T). Figure 4b shows L_{in} as function of the applied bias according to the WAL picture; errors associated to the measurement (included in the graph) are smaller than the actual symbol size, and the dashed line represents a possible trend. We note that L_{in} is approximately 2 orders of magnitude smaller than the mean free path of the sample ($l_c \sim 170$ nm) and grows smaller with the increase in measuring bias. We interpret this as an increasing degree of inelastic scattering as the energy with which the charge carriers are introduced is increased.

Magnetoconductance was further studied as a function of temperature in the lower temperature region ($T < 60$ K).

Figure 4c shows the MC in the range of temperatures between 10 and 40 K, with an applied bias of 100 mV. The MC is still negative overall, and with increasing temperatures fluctuations and few peak-like features start to develop. As before, it was possible to estimate the inelastic scattering length as a function of temperature ($T < 40$ K), as shown in Figure 4d. We find that, below $T = 20$ K, the inelastic mean free path increases marginally with an increase in T . Subsequently, it starts decreasing as T is further increased, suggesting the onset of enhanced phase-breaking inelastic processes as the temperature is increased.

For $T > 40$ K, we found strong evidence of the onset of slow dynamics, reaching its maximum effect around $T = 55$ K. At these temperatures, the cyclic sweep of a magnetic field B (-5 T \leftrightarrow 5 T) gave rise to large (3–4 μS within the full cycle), asymmetric changes in conductance which changed over time scales much larger than experimental time. Cyclic conductance measurements at fixed temperature ($T = 50$ and 60 K) reveals that the amplitude of the first MC measurement cycle was always the largest. This amplitude of MC is reduced in the subsequent cycles. As a result of this, repeated sweeps of B fields did not reproduce the same MCs for the first few sweeps. Gradually, over hours of data acquisition, the MC curves appeared to grow smaller in size. However, it was not possible to apply any meaningful WAL fits. These observations lead us to believe that the phenomenon under investigation is a nonequilibrium process,

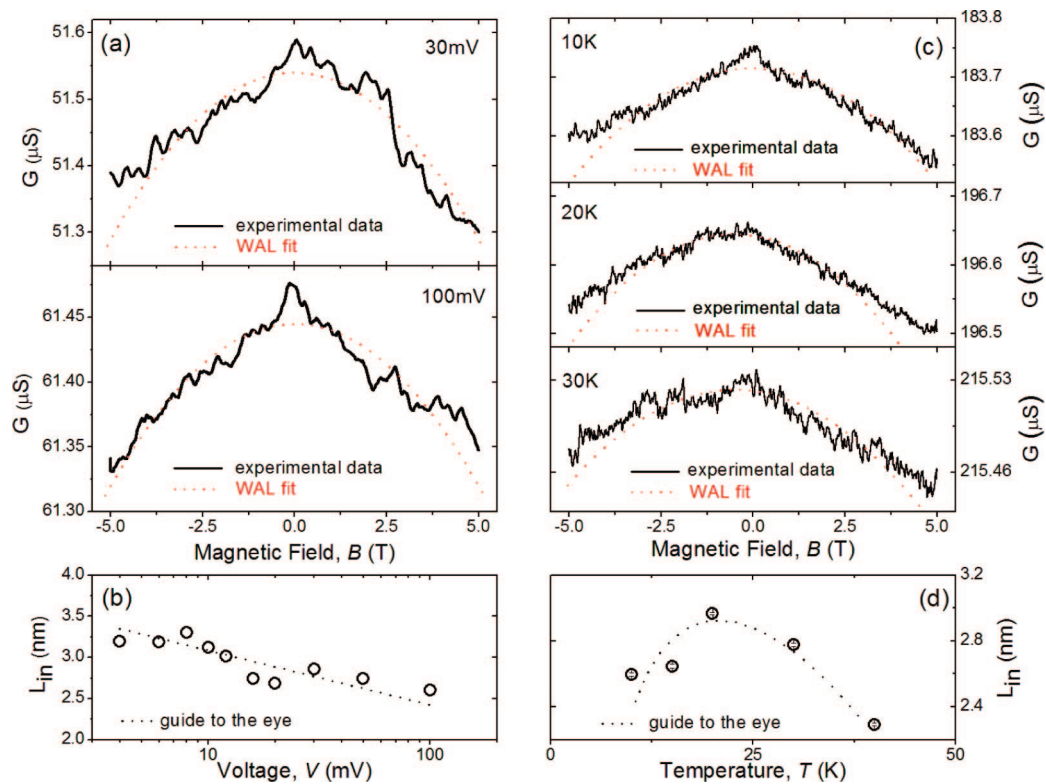


Figure 4. (a) MC and (b) inelastic scattering length, L_{in} , as function of the applied bias. The overall negative MC is due to an enhanced spin-orbit interaction due to the presence of the ferromagnetic clusters. (c) MC and (d) inelastic scattering length as function of the temperature ($T < 45$ K) according to the WAL mechanism. Dashed lines represent fits according to the WAL mechanism. Errors in the estimate of the value of L_{in} are smaller than the size of the symbols.

dominated by slow dynamics sometimes associated with a phase transition.

To bring out the slow dynamics in this temperature region, a detailed study of the conductance was performed as a function of temperature, with different magnetic field exposure histories. Figure 5 shows the low-bias ($V = 1$ mV) temperature dependence of the fractional change in conductance $\Delta G/G_{275\text{K}} = [G(T) - G_{275\text{K}}]/G_{275\text{K}}$, with different B field exposure histories, for $45 \text{ K} < T < 70 \text{ K}$. Curves (a) and (b) represent temperature dependence before (zero-field cooled nm -Co-MWNT) and soon after (zero-field warmed m -Co-MWNT) the device was exposed to a field of $B = 5$ T at $T = 6$ K. Both measurements were performed in a zero magnetic field. A peak-valley feature appeared between 50 and 65 K in measurement (b), as seen in Figure 5. On warming up the sample to room temperature and repeating the measurement after an interval of 1 day under zero magnetic field, the peak-valley feature disappeared completely (curve (c), zero-field cooled nm -Co-MWNT device). When the same measurement was performed under a constant applied magnetic field of $B = 5$ T (field-warmed m -Co-MWNT device), a more prominent and slightly shifted peak-valley feature appeared once again with a trend similar that of to curve (b), as seen in curve (d). The conductance difference and the temperature range between the peak and valley features were larger for the field warmed measurement (d) compared to the zero-field warmed measurement (b). We conclude that the phenomenon responsible for the peak-valley

feature in the conductance of the device depended on the presence, magnitude, and history of magnetic field exposure.

The large time scale changes in the MC around $T = 55$ K, coupled with the sharp drop in L_{in} , and finally the appearance of the peak-valley feature in the presence of a magnetic field around the same temperature suggest that the transport in our hybrid MWNT systems is sensitive to changes in magnetic properties of the underlying nanoclusters. When the magnetization of the individual nanoclusters is randomly oriented, the overall impact appears to average out in the conductance of the host MWNT. However, upon the application of a magnetic field, the nanoclusters will align themselves, and their proximity (< 20 nm) to the wave function of the charge carriers can be expected to give rise to strong local magnetic fields. When a magnetic field is applied, each cluster tends to align its magnetization along with the direction of the field. At low temperatures, this spontaneous magnetization can be retained to a certain extent. However, once the field is turned off, and the sample is warmed up, this magnetization coherence is progressively destroyed due to spin relaxation causing a random reorientation of the spins. And at room temperature, any existing coherent magnetic state is completely destroyed in each cycle. However, since the system is well below the Curie temperature of Co (1388 K),^{40,41} it is difficult to understand why there would be any abrupt magnetic phase change at $T \approx 55$ K, unless we take into account the size of the nanoclusters.

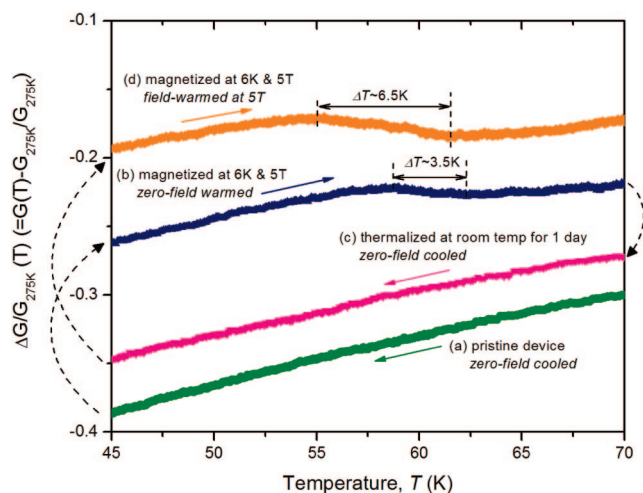


Figure 5. Normalized conductance as function of temperature (45 K < T < 75 K) in a Co filled MWNT device for various magnetization histories. The appearance/disappearance of the “peak–valley” feature indicates the sensitivity of the tube transport properties to the presence, magnitude, and history of magnetic field exposure.

Past works have shown that, at the nanoscale, magnetic particles can be superparamagnetic at room temperature.⁴² Superparamagnetism occurs when nanoscale ferromagnetic clusters undergo a random reorientation of their magnetization due to thermal excitations. As a result, the overall behavior of these clusters appears paramagnetic. Below a certain characteristic temperature, known as the blocking temperature, the ferromagnetic order can be stabilized. The blocking temperature depends on the chemical composition of the nanoparticles, particle size, and the applied magnetic field,^{43–46} and for Co nanoclusters it can be as low as $T \sim 10$ K.⁴⁷ It is possible that our system, which comprises Co nanoclusters with a mean size of ~ 10 nm, undergoes a superparamagnetic transition at about $T \sim 55$ K. The freezing of the ferromagnetic order in such clusters would depend on various factors such as the overall size distribution, their spatial separation, and their interaction with the graphitic matrix of the host MWNT. The occurrence of this phases transition would be spread over a small “window” of temperatures around $T = 55$ K, and its time scale can be affected by the magnitude and speed of the sweeping B field. We propose that the unstable and long time scale magnetoconductance, the dip in the inelastic scattering length above 30 K, and the peak–valley structure seen around $T \sim 55$ K in the G – T curve in the presence of a magnetic field together indicate that (1) the underlying Co nanoclusters are undergoing some kind of phase transition, (2) this is possibly the superparamagnetic to ferromagnetic transition around a blocking temperature of $T \sim 55$ K, and (3) the charge transport in the encapsulating MWNT is sensitive enough to pick up this magnetic transition. A more direct confirmation of this would be to measure the magnetization of these nanostructures as a function of temperature. However, this is currently outside our experimental capabilities.

In conclusion, we have fabricated and investigated the low-temperature transport properties of cobalt cluster embedded

individual MWNTs. We have shown that, in zero magnetic field, the overall electronic transport remains similar to that of bare MWNTs. This is significantly modified under the application of an external magnetic field at low temperatures, with a non-monotonous incremental appearance of discrete states superposed on “unmagnetized” density of states at $T = 6$ K under a magnetic field up to 5 T. Enhanced spin–orbit interaction is believed to be responsible for the overall negative MC observed in our hybrid nanostructures. Most significantly, the signature of a magnetic phase transition is found around $T = 55$ K, which we attribute to the influence of a superparamagnetic to ferromagnetic transition occurring in the underlying ferromagnetic nanoclusters on the overall transport of the host MWNT. Hence, we conclude that the conductance of a MWNT is sensitive to the magnetic activity of nanoscale magnets in its vicinity. Recent theories have predicted that the proximity of ferromagnetic adatoms on the walls of carbon nanotubes may give rise to non-collinear alignment of their magnetizations and hence give rise to non-Heisenberg-like behavior at low dimensions.⁴⁸ Hence, magnetization studies of these systems would be of extreme fundamental interest. These novel hybrid nanostructures open up new avenues of research in fundamental and applied physics and pave the way for increased functionality in carbon nanotube electronics utilizing the magnetic degree of freedom that could give rise to important spintronic applications.

Acknowledgment. We acknowledge financial support from the Interconnect Focus Center New York at RPI, one of the five Focus Center Research Programs of the Semiconductor Research Corporation. S.T. acknowledges the financial support provided by the Office of Research Development and Administration at SIUC through faculty start-up funds. We thank Luca Ortolani and Dr. Sarah Lastella for helpful input in this work.

Supporting Information Available: Preliminary investigation of the low-temperature transport properties of an individual Co–Ni embedded MWNT. This material is available free of charge via the Internet at <http://pubs.acs.org>.

References

- (1) Charlier, J.-C.; Blasé, X.; Roche, S. *Rev. Mod. Phys.* **2007**, *79*, 677.
- (2) Javey, A.; Guo, J.; Wang, Q.; Lundstrom, M.; Dai, H. *Nature* **2003**, *424*, 654.
- (3) Yao, Z.; Postma, H. W. Ch.; Balents, L.; Dekker, C. *Nature* **1999**, *402*, 273.
- (4) Bockrath, M.; Cobden, D. H.; Lu, J.; Rinzler, A. G.; Smalley, R. E.; Balents, L.; McEuen, P. L. *Nature* **1999**, *397*, 598.
- (5) Bockrath, M.; Cobden, D. H.; McEuen, P. L.; Chopra, N. G.; Zettl, A.; Hess, A.; Smalley, R. E. *Science* **1997**, *275*, 1922.
- (6) Kuemmeth, F.; Ilani, S.; Ralph, D. C.; McEuen, P. L. *Nature* **2008**, *452*, 448.
- (7) Tsukagoshi, K.; Alphenaar, B. W.; Ago, H. *Nature* **1999**, *401*, 572.
- (8) Hueso, L. E.; Pruneda, J. M.; Ferrari, V.; Burnell, G.; Valdés-Herrera, J. P.; Simons, B. D.; Littlewood, P. B.; Artacho, E.; Fert, A.; Mathur, N. D. *Nature* **2007**, *445*, 410.
- (9) Sahoo, S.; Kontos, T.; Furer, J.; Hoffmann, C.; Gräber, M.; Cottet, A.; Schönenberger, C. *Nat. Phys.* **2005**, *1*, 99.
- (10) Zhao, B.; Mönch, I.; Vinzelberg, H.; Mühl, T.; Schneider, C. M. *Appl. Phys. Lett.* **2002**, *80*, 3144.
- (11) Odom, T. W.; Huang, J.-L.; Cheung, C. L.; Lieber, C. M. *Science* **2000**, *290*, 1549.

- (12) Guéron, S.; Deshmukh, M. M.; Myers, E. B.; Ralph, D. C. *Phys. Rev. Lett.* **1999**, *83*, 4148.
- (13) Yang, C.-K.; Zhao, J.; Lu, J. P. *Phys. Rev. Lett.* **2003**, *90*, 257203.
- (14) Rahman, M.; Kisaku, M.; Kishi, T.; Roman, T. A.; Diño, W. A.; Nakanishi, H.; Kasai, H. *J. Phys. Soc. Jpn.* **2005**, *74*, 742.
- (15) Wang, J.; Jo, C.; Wu, R. *Appl. Phys. Lett.* **2008**, *92*, 032507.
- (16) Schönenberger, C.; Bachtold, A.; Strunk, C.; Salvétat, J.-P.; Forró, L. *Appl. Phys. A: Mater. Sci. Process.* **1999**, *69*, 283.
- (17) Dresselhaus, M. S.; Dresselhaus, G.; Avouris, Ph. *Carbon Nanotubes: Synthesis, Structure, Properties, and Applications Berlin*; Springer-Verlag: Berlin, 2001.
- (18) Meyer, R. R.; Sloan, J.; Dunin-Borkowski, R. E.; Kirkland, A. I.; Novotny, M. C.; Bailey, S. R.; Hutchison, J. L.; Green, M. L. H. *Science* **2000**, *289*, 1324.
- (19) Leonhardt, A.; Ritschel, M.; Kozhuharova, R.; Graff, A.; Mühl, T.; Huhle, R.; Möncha, I.; Elefant, D.; Schneider, C. M. *Diamond Relat. Mater.* **2003**, *12*, 790.
- (20) Li, D.-C.; Dai, L.; Huang, S.; Mau, A. W. H.; Wang, Z. L. *Chem. Phys. Lett.* **2000**, *316*, 349.
- (21) Hayashi, T.; Hirono, S.; Tomita, M.; Umemura, S. *Nature* **1996**, *381*, 772.
- (22) Guerret-Piécourt, C.; Le Bouar, Y.; Lolseau, A.; Pascard, H. *Nature* **1994**, *372*, 761.
- (23) Yosida, Y.; Shida, S.; Ohsuna, T.; Shiraga, N. *J. Appl. Phys.* **1994**, *76*, 4533.
- (24) Sinha, A. K.; Hwang, D. W.; Hwang, L.-P. *Chem. Phys. Lett.* **2000**, *332*, 455.
- (25) Nolan, P. E.; Lynch, D. C.; Cutler, A. H. *Carbon* **1994**, *32*, 477.
- (26) Harris, P. J. F.; Tsang, S. C. *Chem. Phys. Lett.* **1998**, *293*, 53.
- (27) Mora, C.; Egger, R.; Altland, A. *Semicond. Sci. Technol.* **2006**, *21*, S46.
- (28) Mora, C.; Egger, R.; Altland, A. *Phys. Rev. B* **2007**, *75*, 035310.
- (29) Tarkiainen, R.; Ahlskog, M.; Penttilä, J.; Roschier, L.; Hakonen, P.; Paalanen, M.; Sonin, E. *Phys. Rev. B* **2001**, *64*, 195412.
- (30) Stojetz, B.; Miko, C.; Forró, L.; Strunk, C. *Phys. Rev. Lett.* **2005**, *94*, 186802.
- (31) Ando, T. *J. Phys. Soc. Jpn.* **2005**, *74*, 777.
- (32) Yositate, T. *J. Phys. Soc. Jpn.* **2006**, *75*, 044701.1.
- (33) Langer, L.; Bayot, V.; Grivei, E.; Issi, J.-P.; Heremans, J. P.; Olk, V. H.; Stockman, L.; Van Haesendonck, C.; Bruynseraede, Y. *Phys. Rev. Lett.* **1996**, *76*, 479.
- (34) Song, S. N.; Wang, X. K.; Chang, R. P. H.; Ketterson, J. B. *Phys. Rev. Lett.* **1994**, *72*, 697.
- (35) Lee, P. A.; Ramakrishnan, T. V. *Rev. Mod. Phys.* **1985**, *57*, 287.
- (36) Frydman, A.; Ovadyahu, Z. *Solid State Commun.* **1995**, *94*, 745.
- (37) Kurobe, A.; Kamimura, H. *J. Phys. Soc. Jpn.* **1982**, *51*, 1904.
- (38) Liu, K.; Roth, S.; Düsberg, G. S.; Kim, G. T.; Popa, D.; Mukhopadhyay, K.; Doome, R.; Nagy, J. B. *Phys. Rev. B* **2000**, *61*, 2375.
- (39) Skákalová, V.; Kaiser, A. B.; Woo, Y.-S.; Roth, S. *Phys. Rev. B* **2006**, *74*, 085403.
- (40) Keffer, F. *Handbuch der Physik*; Springer-Verlag: New York, 1966; Vol. 18, Part 2.
- (41) Heller, P. *Rep. Prog. Phys.* **1967**, *30*, 731.
- (42) Hariharan, S.; Gass, J. *Rev. Adv. Mater. Sci.* **2005**, *10*, 398.
- (43) Kwong, H. Y.; Wong, Y. W.; Wong, K. H. *J. Appl. Phys.* **2007**, *102*, 114303.
- (44) Romanus, E.; Matoussevitch, N.; Prass, S.; Heinrich, J.; Müller, R.; Berkov, D. V.; Bönnemann, H.; Weber, P. *Appl. Organomet. Chem.* **2004**, *18*, 548.
- (45) Klimenkov, M.; von Borany, J.; Matz, D.; Eckert, D.; Wolf, M.; Müller, K.-H. *Appl. Phys. A: Mater. Sci. Process.* **2002**, *74*, 571.
- (46) Zhang, Y. D.; Budnick, J. I.; Hines, C. L. C.; Xiao, J. Q. *Appl. Phys. Lett.* **1998**, *72*, 2053.
- (47) Respaud, M.; Broto, J. M.; Rakoto, H.; Fert, A. R.; Thomas, L.; Barbara, B.; Verelst, M.; Snoeck, E.; Lecante, P.; Mosset, A. *Phys. Rev. B* **1998**, *57*, 2925.
- (48) Costa, A. T.; Rocha, C. G.; Ferreira, M. S. *Phys. Rev. B* **2007**, *76*, 085401.

NL802456T